RSC Advances

PAPER

View Article Online
View Journal | View Issue

Open Access Article. Published on 19 November 2019. Downloaded on 12/9/2025 12:19:22 AM.
This article is licensed under a Creative Commons Attribution-NonCommercial 3.0 Unported Licence.

Check for updates

Cite this: *RSC Adv.*, 2019, **9**, 37747

Molecular design and properties of bridged energetic pyridines derivatives†

Diandian Zhai, Jinpeng Wang, Lina Hao, Congming Ma,* Peng Ma,* Yong Pan* and Juncheng Jiang

A series of bridged pyridine-based energetic derivatives were designed and their geometrical structures, electronic structures, heats of formation, detonation properties, thermal stabilities, thermodynamic properties and electrostatic potential were fully investigated using density functional theory. The results show that the steric hindrance effect is a decisive factor for structural stability, and the formation of intramolecular or intermolecular hydrogen bonds doesn't provide advantages to stabilize molecular structure, which was demonstrated by insertion of 3,4,5-trinitro-1*H*-pyrazole, 3,4-dinitro-1*H*-pyrazol-5-amine, 3,5-dinitro-1*H*-pyrazol-4-amine and 3-nitro-1*H*-1,2,4-triazol-5-amine. The azide group and azo bridge play an important role in improving the heats of formation of energetic pyridine-based materials. All designed molecules were found to have values of density ranging from 1.70 g cm^{-3} (**E6**, **F6**) to 2.11 g cm^{-3} (**D3**), values of detonation velocity ranging from 7.1 km s^{-1} (**F1**) to 9.77 km s^{-1} (**D8**), and values of detonation pressure ranging from 21.5 GPa (**F1**) to 46.0 GPa (**D8**). When a p-π conjugation formed between the nitrogen atom and pyridine ring, the bond between nitrogen and hydrogen atoms may be broken as the trigger bond.

Received 4th September 2019
Accepted 7th November 2019

DOI: 10.1039/c9ra07087g

rsc.li/rsc-advances

1 Introduction

Compared with carbocyclic aromatic energetic compounds, nitrogen heterocyclic nitro compounds have higher density and better detonation performance. However, the difficulty of synthesizing some nitro heteroaromatic systems may attributed to their electron deficiency, making electrophilic aromatic substitution problematic.[1] By the addition of electron donation substituents to the heteroaromatic ring, especially the amino group, nitration may proceed relatively smoothly. Additionally, high-nitrogen materials, which have large numbers of N–N and C–N bonds and few or no nitro groups, typically gain energy from their very high positive heats of formation rather than from the conventional organic energetic materials oxidizing the carbon in the backbone to carbon dioxide. Meanwhile, due to their lower carbon and hydrogen content, some properties of high-nitrogen such as density and oxygen balance have distinct advantages over conventional energetic materials.[2] As a result of these properties, scientists have designed and synthesized energetic azo materials with useful detonation properties. Licht and Ritter[3,4] reported the synthesis of 2,4,6-trinitropyridine (TNPy), 2,4,6-trinitropydine-1-oxide (TNPyO) and 2,6-diamino-3,5-dinitropyridine-1-oxide (ANPyO) in the twentieth century, illustrating that the density and thermal stability increase with an alternating array of amino- and nitro-groups. Zhao[5] reported two promising heat-resistant energetic materials based on the pyridine and tetrazole ring were synthesized with a high decomposition temperature in excess of 300 °C. Recently, a kind of azo-bridged pyridine precursor was synthesized for the first time to develop new energetic pyridine-based compounds.[6] Thus, this lead to the attempt to design and calculate bridged energetic pyridines derivatives (Scheme 1).

In this study, a systematic research on electronic structures, heats of formation (HOF), detonation properties, thermal stabilities and thermodynamic properties of bridged energetic pyridines derivatives (such as –C=C–, –NH–NH– and –N=N–)

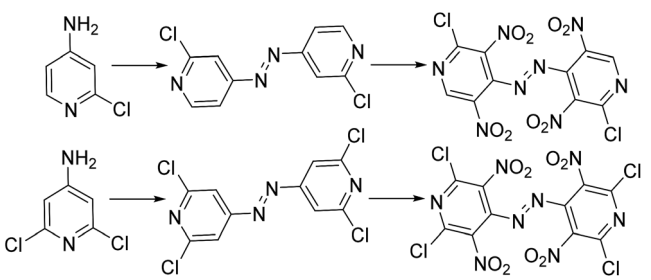

Scheme 1 Template reactions of energetic pyridine molecules.

College of Safety Science and Engineering, Nanjing Tech University, Nanjing, Jiangsu, CN 211800, China. E-mail: maming1306@126.com; mpcctv@163.com; lh1083517594@gmail.com

† Electronic supplementary information (ESI) available: Computational methods, DFT/B3LYP/6-311G(d,p) optimized geometries of **B9**, **B10**, **B11** and **B12**; the specific data of bond order for all designed compounds. See DOI: 10.1039/c9ra07087g

Open Access Article. Published on 19 November 2019. Downloaded on 12/9/2025 12:19:22 AM.
This article is licensed under a Creative Commons Attribution-NonCommercial 3.0 Unported Licence.

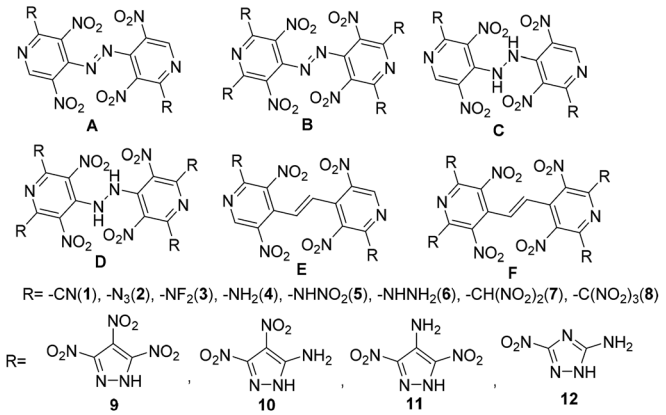

Scheme 2 Designed energetic molecules based on bridged pyridines.

with various energetic groups (such as –CN, $-N_3$, $-NF_2$, $-NH_2$, $-NHNO_2$, $-NHNH_2$, $-CH(NO_2)_2$, $-C(NO_2)_3$)[7] or common energetic materials containing active hydrogen atoms (such as 3,4,5-trinitro-1*H*-pyrazole, 3,4-dinitro-1*H*-pyrazol-5-amine, 3,5-dinitro-1*H*-pyrazol-4-amine, and 3-nitro-1*H*-1,2,4-triazol-5-amine) were investigated (Scheme 2, series **A–F**). It is certain that all results will provide useful information for a better understanding of the physical and chemical properties of energetic pyridines.

2 Results and discussion

2.1 Electronic structures

The Highest Occupied Molecular Orbital (HOMO) and the Lowest Unoccupied Molecular Orbital (LUMO), which is called Frontier Molecular Orbital Theory (FMO Theory), has

Table 1 Calculated HOMO and LUMO energies (eV) and energy gaps ($\Delta E_{LUMO-HOMO}$) of designed compounds

	A1	A2	A3	A4	A5	A6	A7	A8	A9	A10	A11	A12
HOMO	−8.67	−7.90	−8.28	−7.32	−8.34	−7.30	−8.75	−8.80	−8.91	−7.73	−7.45	−7.78
LUMO	−5.08	−4.41	−4.49	−4.04	−4.84	−4.09	−5.19	−5.22	−5.37	−4.88	−4.78	−5.23
$\Delta E_{HOMO-LUMO}$	3.59	3.49	3.79	3.28	3.50	3.21	3.56	3.58	3.54	2.85	2.67	2.55
	B1	**B2**	**B3**	**B4**	**B5**	**B6**	**B7**	**B8**	**B9**	**B10**	**B11**	**B12**
HOMO	−9.27	−7.59	−8.78	−6.80	−8.39	−6.45	−9.30	−9.39	−9.25	−7.88	−7.50	−7.73
LUMO	−5.66	−4.44	−5.49	−3.54	−4.95	−3.54	−5.72	−5.80	−5.73	−5.54	−4.87	−5.67
$\Delta E_{HOMO-LUMO}$	3.61	3.15	3.29	3.26	3.44	2.91	3.58	3.59	3.52	2.34	2.63	2.06
	C1	**C2**	**C3**	**C4**	**C5**	**C6**	**C7**	**C8**	**C9**	**C10**	**C11**	**C12**
HOMO	−8.48	−7.78	−8.26	−7.15	−8.07	−6.83	−8.50	−8.66	−8.85	−7.64	−7.36	−7.86
LUMO	−4.23	−3.48	−3.96	−3.18	−4.10	−3.17	−4.42	−4.59	−4.51	−4.06	−3.99	−4.41
$\Delta E_{HOMO-LUMO}$	4.25	4.30	4.30	3.97	3.97	3.66	4.08	4.07	4.34	3.58	3.37	3.45
	D1	**D2**	**D3**	**D4**	**D5**	**D6**	**D7**	**D8**	**D9**	**D10**	**D11**	**D12**
HOMO	−8.97	−7.50	−8.69	−6.77	−8.15	−6.82	−9.13	−9.21	−9.18	−7.84	−7.27	−7.63
LUMO	−4.81	−3.40	−4.24	−2.82	−4.23	−2.95	−5.02	−5.24	−5.28	−4.59	−4.28	−4.46
$\Delta E_{HOMO-LUMO}$	4.16	4.10	4.45	3.95	3.92	3.87	4.11	3.97	3.90	3.25	2.99	3.17
	E1	**E2**	**E3**	**E4**	**E5**	**E6**	**E7**	**E8**	**E9**	**E10**	**E11**	**E12**
HOMO	−8.71	−7.89	−8.73	−7.15	−8.23	−7.01	−8.71	−8.77	−8.95	−7.66	−7.40	−7.51
LUMO	−4.42	−3.78	−4.33	−3.25	−3.88	−3.03	−4.23	−4.40	−4.59	−4.15	−4.09	−3.84
$\Delta E_{HOMO-LUMO}$	4.29	4.11	4.40	3.90	4.35	3.98	4.48	4.37	4.36	3.51	3.31	3.67
	F1	**F2**	**F3**	**F4**	**F5**	**F6**	**F7**	**F8**	**F9**	**F10**	**F11**	**F12**
HOMO	−9.22	−7.60	−8.92	−6.73	−8.22	−6.77	−9.30	−9.35	−9.20	−7.88	−7.46	−7.57
LUMO	−4.77	−3.63	−4.31	−2.78	−4.02	−2.91	−4.91	−5.12	−5.18	−4.50	−4.23	−4.55
$\Delta E_{HOMO-LUMO}$	4.45	3.97	4.61	3.94	4.20	3.86	4.39	4.23	4.02	3.38	3.23	3.02

Open Access Article. Published on 19 November 2019. Downloaded on 12/9/2025 12:19:22 AM.
This article is licensed under a Creative Commons Attribution-NonCommercial 3.0 Unported Licence.

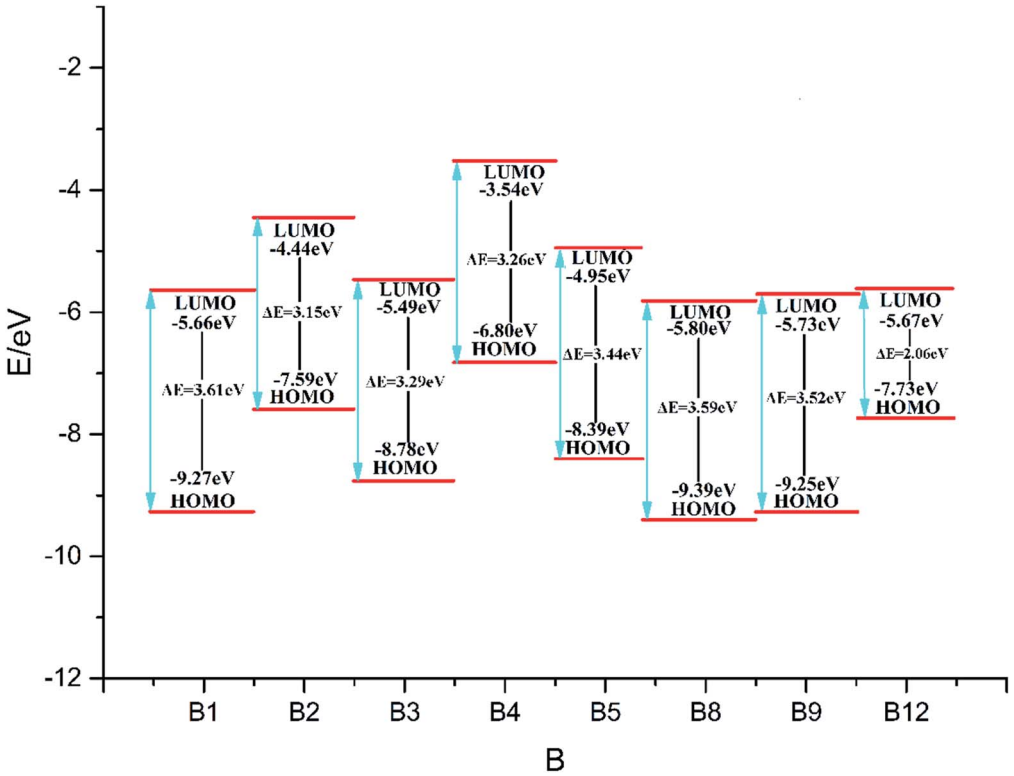

Fig. 1 The variation trends of $\Delta E_{\mathrm{LUMO-HOMO}}$ of representative designed compounds.

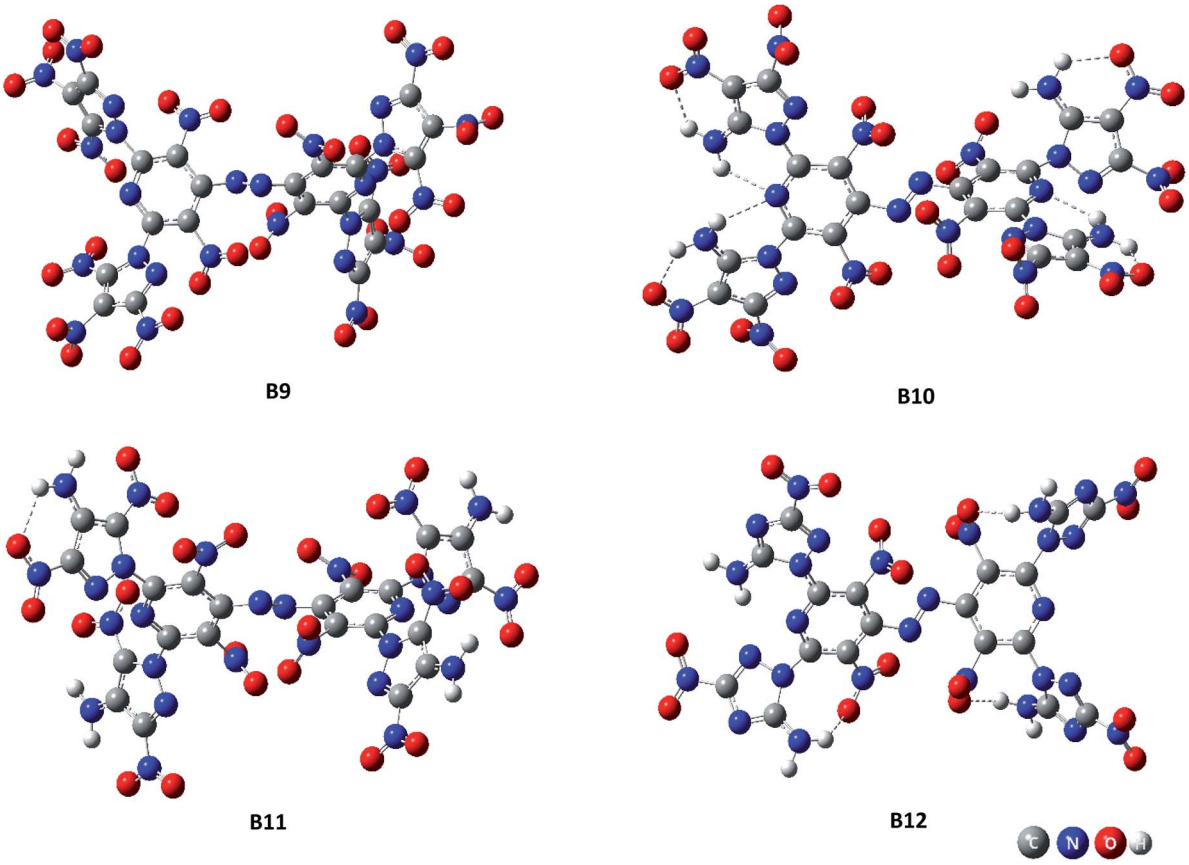

Fig. 2 Spatial structures of representative compounds B9–B12.

Open Access Article. Published on 19 November 2019. Downloaded on 12/9/2025 12:19:22 AM.
This article is licensed under a Creative Commons Attribution-NonCommercial 3.0 Unported Licence.

crucial effects on reaction mechanisms. Particularly, their energy gap can provide many useful information on optical polarizability, kinetic stability and chemical reactivity.[8] The frontier molecular orbital energies and their energy gaps ($\Delta E_{LUMO-HOMO}$) for designed compounds were listed in Table 1. For homologous bridged pyridine derivatives, it is found that HOMO energy levels increase evidently while $-NH_2$ and $-NHNH_2$ groups are introduced to the pyridine ring, so as LUMO energy levels. Oppositely, HOMO energy levels decrease when –CN, $-CH(NO_2)_2$, $-C(NO_2)_3$ or 3,4,5-trinitro-1*H*-pyrazole are attached, so as LUMO energy levels. Furthermore, HOMO and LUMO energy levels present no regularity when different bridges (such as –CH=CH–, –NH–NH– and –N=N–) are incorporated.

Fig. 1 (the HOMO–LUMO pictures are in ESI Table S1†) displays the variation trends of highest occupied orbital, lowest unoccupied molecular orbital energy levels and energy gaps of representative designed compounds **B1**, **B2**, **B3**, **B4**, **B5**, **B8**, **B9**, **B12**. It reveals that $\Delta E_{LUMO-HOMO}$ decreases evidently while 3,4-dinitro-1*H*-pyrazol-5-amine (**10**), 3,5-dinitro-1*H*-pyrazol-4-amine (**11**), and 3-nitro-1*H*-1,2,4-triazol-5-amine (**12**) are incorporated for series **A–F**, whereas the addition of other groups or energetic compounds makes similar contributions to $\Delta E_{LUMO-HOMO}$. Surprisingly, $\Delta E_{LUMO-HOMO}$ is demonstrated to be much higher when 3,4,5-trinitro-1*H*-pyrazole (**9**) was incorporated than that of other three energetic compounds (**10–12**), convincing that steric hindrance effect is a decisive factor for structural stability caused by a combination of amino and nitro groups (Fig. 2, see ESI Table S2†). In general, $\Delta E_{LUMO-HOMO}$ increases gradually as different bridges incorporated in order of –N=N–, –NH–NH–, –CH=CH–. In view of all designed compounds, compound **F3** has the highest $\Delta E_{LUMO-HOMO}$ of 4.61 eV while compounds **B12** has the smallest $\Delta E_{LUMO-HOMO}$ of 2.06 eV, showing that **F3** is the most inactive and **B12** is the most active under external stimulus.

$$CH_3CH(NO_2)_2 + 2CH_4 \longrightarrow CH_3CH_3 + 2CH_3NO_2$$
$$CH_3C(NO_2)_3 + 3CH_4 \longrightarrow CH_3CH_3 + 3CH_3NO_2$$

Scheme 3 Isodesmic reactions for polynitromethane.

Table 2 HOF calculated for polynitromethane at G4 level

Compd	E_0[a] (a.u.)	ZPE[a] (kJ mol^{-1})	H_T[a] (kJ mol^{-1})	$\Delta H_{f,gas}$ (kJ mol^{-1})
CH_4	−40.506540	117.5	10.0	−74.6[b]
CH_3CH_3	−79.808058	195.7	11.6	−84.0[b]
CH_3NO_2	−244.957724	130.7	14.0	−81.0[b]
$CH_3CH(NO_2)_2$	−488.711186	212.5	22.9	−105.1[c]
$CH_3C(NO_2)_3$	−693.145352	216.1	29.3	−73.9[c]

[a] Calculated at the G4 level. [b] Obtained from http://webbook.nist.gov. [c] Obtained by isodesmic reaction.

2.2 Heat of formation

Heat of formation (HOF), calculated by atomization reaction or isodesmic reaction, is an important parameter in predicting detonation properties of energetic materials. Compounds $CH_3CH(NO_2)_2$ and $CH_3C(NO_2)_3$ were calculated *via* isodesmic reactions (Scheme 3) at G4 level (Table 2). Total energies, zero-point energies, and thermal corrections for the reference compounds using the isodesmic reactions (Scheme S1, see ESI†) are listed in Table 3.

Table 4 presents the $\Delta H_{f,gas}$, A, ν, σ_{tot}^2, ΔH_{sub} and $\Delta H_{f,solid}$ of bridged pyridine derivatives. It is seen that all compounds have positive $\Delta H_{f,gas}$ range from to 142.8 (**F4**) to 1876.9 kJ mol^{-1} (**B2**). It reveals that energetic materials attached with $-N_3$ group often have the highest $\Delta H_{f,solid}$, while $-NH_2$, $-CH(NO_2)_2$, $-NHNO_2$ groups are not conducive to improvement of $\Delta H_{f,solid}$. For each series **F**, the influence of different energetic groups on $\Delta H_{f,solid}$ can be described as the following order: $-N_3$ > –CN > 3,4,5-trinitro-1*H*-pyrazole > 3-nitro-1*H*-1,2,4-triazol-5-amine > 3,5-dinitro-1*H*-pyrazol-4-amine > 3,4-dinitro-1*H*-pyrazol-5-amine > $-NHNH_2$ > $-NF_2$ > $-C(NO_2)_3$ > $-NHNO_2$ > $-CH(NO_2)_2$ > $-NH_2$. Meanwhile, azo bridged pyridine derivatives usually have better HOFs than

Table 3 Calculated total energies (E_0), zero-point energies (ZPE), thermal corrections (H_T) and heats of formation (HOFs) of the reference compounds

Compd	E_0[a] (a.u.)	ZPE[b] (kJ mol^{-1})	H_T[b] (kJ mol^{-1})	$\Delta H_{f,gas}$ (kJ mol^{-1})
CH_4	−40.541022	115.8	10.1	−74.6[c]
NH_3	−56.589815	89.1	10.1	−45.9[c]
CH_3NO_2	−245.127760	128.9	11.7	−81.0[c]
CH_3CN	−132.816078	117.4	12.0	74.0[c]
CH_3N_3	−204.186410	130.3	14.3	293.4 (ref. 9)
CH_3NF_2	−294.351870	121.4	13.7	−98.0[d]
CH_3NH_2	−95.908614	165.7	11.5	−23.5[c]
CH_3NHNO_2	−300.491413	174.6	16.1	−73.2 (ref. 10)
CH_3NHNH_2	−151.253386	211.3	13.5	94.5[c]
$CH_3CH(NO_2)_2$	−489.043812	210.0	23.0	−105.1[e]
$CH_3C(NO_2)_3$	−693.610990	213.7	29.4	−73.9[e]
$CH_3N{=}NCH_3$	−189.363781	218.2	16.1	146.0[d]
$CH_3NHNHCH_3$	−190.578383	282.9	17.1	90.0 (ref. 11)
$CH_3CH{=}CHCH_3$	−157.306017	278.9	17.0	−10.8[c]
	−248.398244	229.8	13.8	140.6 (ref. 12)
	−226.304546	184.6	12.4	177.4 (ref. 12)
	−242.358564	155.0	11.9	192.7 (ref. 13)

[a] Calculated at the B3LYP/def2-TZVPP level. [b] Calculated at the B3LYP/6-311G(d,p) level, and the scaling factor is 0.9888 for ZPE and 1.0062 for H_T.[14] [c] Obtained from http://webbook.nist.gov. [d] Calculated at G4 level. [e] Obtained by isodesmic reaction.

Open Access Article. Published on 19 November 2019. Downloaded on 12/9/2025 12:19:22 AM.
This article is licensed under a Creative Commons Attribution-NonCommercial 3.0 Unported Licence.

hydrazine or vinyl bridged compounds. This phenomenon may be caused by π–π conjugated system and large amount of nitrogen content. Besides, these high positive HOFs make great contribution to increasing detonation properties such as detonation velocities and detonation pressures.

2.3 Detonation property

Detonation properties that related to oxygen balance (OB), density (ρ), heat of detonation (Q), detonation velocity (D) and detonation pressure (P) are summarized in Table 5. For a comparison, detonation properties of two well-known explosives 1,3,5-trinitro-1,3,5-triazinane (**RDX**) and 1,3,5,7-tetranitro-1,3,5,7-tetrazocane (**HMX**) were also presented. It is seen that most of the designed compounds have negative OB, and energetic materials attached with $-C(NO_2)_3$ group always have OB of nearly zero, proving that polynitro compounds contribute to good values of OB. Meanwhile, energetic materials attached with –CN, $-NH_2$, or $-NHNH_2$ group always have dissatisfied OB, proving that cyano and amino compounds are not conducive to good oxygen balance. Bridged pyridine derivatives with different substituents were also found to have different ρ, Q, D and P values: values of ρ range from 1.70 (**E6**, **F6**) to 2.11 g cm^{-3} (**D3**); values of Q range from 1090.5 (**D4**) to 1769.2 cal g^{-1} (**B3**). Compound **F1** has the smallest value of detonation velocity (7.1 km s^{-1}) and detonation pressure (21.5 GPa), while Compound **D8** has the highest value of detonation velocity (9.77 km s^{-1}) and detonation pressure (46.0 GPa), which is also better than that of **RDX** and **HMX**.

Fig. 3 displays variation trends of ρ, Q, D and P of designed compounds, in which Fig. 3a shows the influence of different energetic groups on density. It can be seen that

Table 4 Calculated molecular properties and heats of formation of the designed compounds

Compd	$\Delta H_{f,gas}$ (kJ mol^{-1})	A (Å^2)	ν	σ_{tot}^2 (kcal mol^{-1})^2	ΔH_{sub} (kJ mol^{-1})	$\Delta H_{f,solid}$ (kJ mol^{-1})	Compd	$\Delta H_{f,gas}$ (kJ mol^{-1})	A (Å^2)	ν	σ_{tot}^2 (kcal mol^{-1})^2	ΔH_{sub} (kJ mol^{-1})	$\Delta H_{f,solid}$ (kJ mol^{-1})
A1	929.7	361.4	0.1629	168.3	194.5	735.2	**D1**	1102.5	382.9	0.1418	268.6	218.9	883.7
A2	1209.7	380.5	0.2410	109.4	209.6	1000.1	**D2**	1671.6	420.8	0.2479	114.2	246.9	1424.6
A3	602.9	353.6	0.1600	141.1	184.9	418.1	**D3**	467.3	387.8	0.0520	230.6	204.4	263.0
A4	471.3	336.8	0.2254	167.6	181.6	289.7	**D4**	145.6	344.2	0.2484	233.9	197.4	−51.8
A5	560.6	395.8	0.1514	139.3	219.2	341.5	**D5**	339.4	455.4	0.1536	186.9	281.1	58.3
A6	726.8	366.9	0.2431	129.2	201.5	525.3	**D6**	653.6	402.8	0.2463	190.3	241.0	412.6
A7	558.4	450.2	0.0975	197.1	269.1	289.3	**D7**	360.2	558.5	0.0774	310.9	394.8	−34.6
A8	687.8	477.7	0.0678	170.4	290.8	397.0	**D8**	628.3	612.6	0.0363	230.8	451.6	176.7
A9	1178.8	586.4	0.1231	185.8	429.6	749.2	**D9**	1616.9	836.3	0.0712	259.5	823.3	793.6
A10	971.9	553.6	0.1878	212.4	398.4	573.5	**D10**	1216.5	762.0	0.1238	309.5	703.8	512.7
A11	984.5	554.5	0.2110	136.2	392.9	591.6	**D11**	1217.2	765.3	0.2059	173.1	708.0	509.2
A12	1065.4	502.7	0.2232	275.0	348.9	716.5	**D12**	1300.3	662.0	0.1805	276.2	550.8	749.5
B1	1296.9	407.9	0.1216	228.3	234.7	1062.2	**E1**	721.7	362.8	0.1804	166.8	197.3	524.4
B2	1876.9	443.0	0.2402	120.6	268.8	1608.1	**E2**	1069.3	377.9	0.2073	123.5	206.9	862.4
B3	640.6	391.9	0.1404	199.4	220.5	420.0	**E3**	403.0	373.6	0.0909	149.6	193.8	209.2
B4	357.9	355.9	0.2413	238.0	206.2	151.6	**E4**	276.0	337.8	0.2483	163.3	183.9	92.2
B5	536.8	472.8	0.1331	169.2	295.0	241.8	**E5**	348.5	389.7	0.1862	139.7	217.3	131.2
B6	891.6	417.0	0.2386	240.8	259.0	632.5	**E6**	546.4	363.6	0.2475	215.8	210.5	335.8
B7	552.3	581.1	0.0696	260.6	419.1	133.2	**E7**	347.6	442.0	0.1104	190.9	262.4	85.2
B8	806.7	630.5	0.0344	149.4	472.2	334.5	**E8**	467.4	473.0	0.0801	188.2	289.2	178.2
B9	1814.7	846.4	0.0712	230.2	840.7	974.0	**E9**	972.7	587.0	0.1287	185.3	431.1	541.6
B10	1409.3	787.7	0.1153	294.7	745.8	663.5	**E10**	761.8	551.8	0.2108	199.5	397.3	364.5
B11	1405.2	785.0	0.1988	145.8	738.1	667.1	**E11**	779.7	555.4	0.2176	132.8	394.1	385.5
B12	1516.2	682.2	0.1962	287.5	584.1	932.1	**E12**	804.2	492.1	0.2362	212.1	331.8	472.4
C1	721.6	338.5	0.1841	168.0	178.8	542.8	**F1**	1091.1	408.8	0.1271	247.8	237.9	853.2
C2	999.7	359.1	0.2373	107.7	191.4	808.4	**F2**	1695.3	440.8	0.2272	116.2	265.0	1430.3
C3	397.5	343.4	0.1063	154.4	172.2	225.3	**F3**	424.6	415.5	0.0629	186.3	228.9	195.7
C4	259.5	324.5	0.2353	169.9	173.7	85.8	**F4**	142.8	352.2	0.2493	251.6	205.7	−62.8
C5	355.4	382.8	0.1629	163.8	211.8	143.6	**F5**	322.2	462.1	0.1698	167.2	287.7	34.5
C6	514.5	354.0	0.2483	149.5	194.5	320.0	**F6**	652.5	411.1	0.2499	199.3	249.9	402.6
C7	356.8	434.7	0.1005	209.7	255.2	101.6	**F7**	354.2	564.8	0.0749	288.0	400.8	−46.6
C8	475.9	422.2	0.0799	155.9	235.9	240.0	**F8**	581.1	624.6	0.0348	187.7	465.9	115.2
C9	974.1	570.3	0.1266	219.4	412.1	562.0	**F9**	1601.7	852.6	0.0711	249.0	853.6	748.1
C10	754.5	531.4	0.2053	190.4	371.0	383.5	**F10**	1206.4	794.9	0.1198	297.1	759.5	446.9
C11	783.0	538.4	0.2094	162.9	376.5	406.5	**F11**	1195.9	789.0	0.2009	142.8	744.9	451.0
C12	852.1	469.9	0.2191	274.5	312.6	539.5	**F12**	1278.2	676.5	0.2042	227.0	570.7	707.5

[a] Calculated at the B3LYP/def2-TZVPP level. [b] Calculated at the B3LYP/6-311G(d,p) level, and the scaling factor is 0.9888 for ZPE and 1.0062 for H_T.[14]

Open Access Article. Published on 19 November 2019. Downloaded on 12/9/2025 12:19:22 AM.
This article is licensed under a Creative Commons Attribution-NonCommercial 3.0 Unported Licence.

Table 5 Predicted densities (ρ), heats of detonation (Q), detonation velocities (D)

Compd	Q (cal g^{-1})	D (km s^{-1})	P (GPa)	ρ (g cm^{-3})	OB (%)	Compd	Q (cal g^{-1})	D (km s^{-1})	P (GPa)	ρ (g cm^{-3})	OB (%)
A1	1470.6	7.75	26.3	1.76	−65.7	**D2**	1483.0	8.55	33.0	1.85	−39.2
A2	1515.0	8.32	30.8	1.81	−46.6	**D3**	1709.2	8.76	37.2	2.11	−36.5
A3	1649.6	8.46	33.4	1.97	−44.6	**D4**	1090.5	7.67	25.9	1.78	−63.8
A4	1321.9	7.89	27.3	1.77	−60.9	**D5**	1428.1	9.05	38.0	1.94	−18.5
A5	1486.5	8.66	34.0	1.87	−33.0	**D6**	1249.7	7.95	27.6	1.75	−62.5
A6	1397.7	8.03	28.1	1.75	−60.3	**D7**	1593.9	9.26	40.0	1.96	−14.3
A7	1585.6	8.84	35.7	1.89	−28.0	**D8**	1730.9	9.77	46.0	2.08	5.0
A8	1684.6	9.44	41.8	1.99	−12.1	**D9**	1624.9	9.18	39.5	1.99	−17.8
A9	1608.9	8.89	36.5	1.93	−27.1	**D10**	1402.3	8.54	33.6	1.92	−38.1
A10	1439.7	8.40	32.1	1.88	−43.0	**D11**	1402.4	8.54	33.5	1.92	−38.1
A11	1444.0	8.39	31.9	1.87	−43.0	**D12**	1277.3	8.20	30.5	1.87	−45.7
A12	1376.6	8.16	29.9	1.83	−49.2	**E1**	1383.2	7.20	22.3	1.71	−85.4
B1	1478.0	7.57	25.0	1.75	−68.9	**E2**	1470.5	7.86	27.1	1.76	−64.8
B2	1561.2	8.59	33.1	1.84	−36.3	**E3**	1577.0	7.87	28.2	1.89	−62.0
B3	1769.2	8.75	37.1	2.10	−33.8	**E4**	1237.1	7.32	23.1	1.72	−81.6
B4	1189.8	7.78	26.7	1.78	−60.3	**E5**	1409.8	8.17	29.8	1.82	−49.8
B5	1493.1	9.10	38.3	1.94	−15.9	**E6**	1327.6	7.51	24.2	1.70	−79.6
B6	1350.1	8.05	28.1	1.74	−59.5	**E7**	1521.7	8.43	32.1	1.85	−42.1
B7	1643.1	9.28	40.1	1.96	−12.3	**E8**	1626.2	9.04	37.9	1.94	−24.2
B8	1767.7	9.77	45.9	2.08	6.7	**E9**	1562.7	8.57	33.5	1.89	−37.7
B9	1659.0	9.21	39.8	1.99	−16.4	**E10**	1387.8	8.07	29.3	1.84	−54.5
B10	1438.7	8.55	33.6	1.91	−36.6	**E11**	1393.9	8.05	29.1	1.83	−54.5
B11	1437.7	8.57	33.8	1.92	−36.6	**E12**	1297.3	7.79	27.0	1.81	−62.3
B12	1327.0	8.24	30.7	1.86	−44.0	**F1**	1401.2	7.08	21.5	1.70	−86.5
C1	1369.9	7.69	26.0	1.77	−69.2	**F2**	1505.1	8.17	29.5	1.79	−51.7
C2	1420.3	8.26	30.4	1.82	−50.0	**F3**	1703.3	8.25	32.4	2.04	−48.0
C3	1560.6	8.41	33.1	1.97	−47.8	**F4**	1099.2	7.23	22.6	1.73	−79.6
C4	1214.7	7.78	26.6	1.78	−64.6	**F5**	1430.7	8.69	34.5	1.90	−29.2
C5	1401.6	8.59	33.5	1.87	−36.2	**F6**	1259.6	7.57	24.5	1.70	−76.3
C6	1297.3	7.94	27.6	1.76	−63.8	**F7**	1600.3	9.00	37.4	1.93	−22.6
C7	1514.9	8.80	35.4	1.90	−30.6	**F8**	1726.3	9.75	45.4	2.05	−1.7
C8	1619.5	9.46	42.3	2.01	−14.5	**F9**	1627.4	8.98	37.6	1.96	−23.3
C9	1555.1	8.84	36.1	1.93	−29.2	**F10**	1405.3	8.30	31.4	1.88	−44.3
C10	1377.5	8.37	31.9	1.89	−45.2	**F11**	1402.9	8.32	31.6	1.89	−44.3
C11	1387.1	8.34	31.5	1.87	−45.2	**F12**	1277.1	7.97	28.5	1.84	−53.3
C12	1307.4	8.10	29.5	1.84	−51.6	**RDX**[15]	1590.7	8.75	34.0	1.82	−21.6
D1	1395.1	7.54	25.0	1.77	−72.1	**HMX**[15]	1633.9	9.10	39.0	1.91	−21.6

compounds substituted by $-NF_2$ group have the highest density while –CN, $-NH_2$ or $-NHNH_2$ substituted ones have smaller density. Compounds with different bridged groups have similar values in detonation velocity, detonation pressure and density, indicating that –CH=CH–, –NH–NH– and –N=N– bridged groups have little effect in improving the values of ρ, Q, D and P. Fig. 3b shows the influence of different energetic groups on Q. It can be seen that compounds substituted by $-NF_2$ and $-C(NO_2)_3$ group have the highest heat of detonation while $-NH_2$, $-NHNH_2$ and 3-nitro-1*H*-1,2,4-triazol-5-amine substituted ones have smaller heat of detonation. It is clearly seen that different bridged groups have different effects on Q values in the order of –N=N–, –CH=CH–, –CH=CH–.

In view of Fig. 3c and d, it is seen that the influence of different energetic groups on values of D and P were approximately the same throughout all series. The general influence order of different energetic groups on values of D and P can be described as follows: $-C(NO_2)_3$ > $-CH(NO_2)_2$ ≈ 3,4,5-trinitro-1*H*-pyrazole > $-NHNO_2$ > $-NF_2$ ≈ $-N_3$ ≈ 3,4-dinitro-1*H*-pyrazol-5-amine ≈ 3,5-dinitro-1*H*-pyrazol-4-amine > $-NHNH_2$ > $-NH_2$ > –CN while the influence of different bridges on values of D and P can be described in the order of –N=N– ≈ –NH–NH– > –CH=CH–. It can be concluded that polynitro groups are the most effective groups in improving D and P values while it is on the opposite side for insertion of –CN, $-NH_2$ and $-NHNH_2$.

2.4 Thermal stability

The bond dissociation energies (BDEs) are important in understanding thermal stability and enhancing controllability of kinetic energy release. In general, the smaller the energy is needed for breaking a bond, the weaker the bond is, and thus, this chemical bond may be acted as the trigger bond. The possible trigger bond with the weakest

Open Access Article. Published on 19 November 2019. Downloaded on 12/9/2025 12:19:22 AM.
This article is licensed under a Creative Commons Attribution-NonCommercial 3.0 Unported Licence.

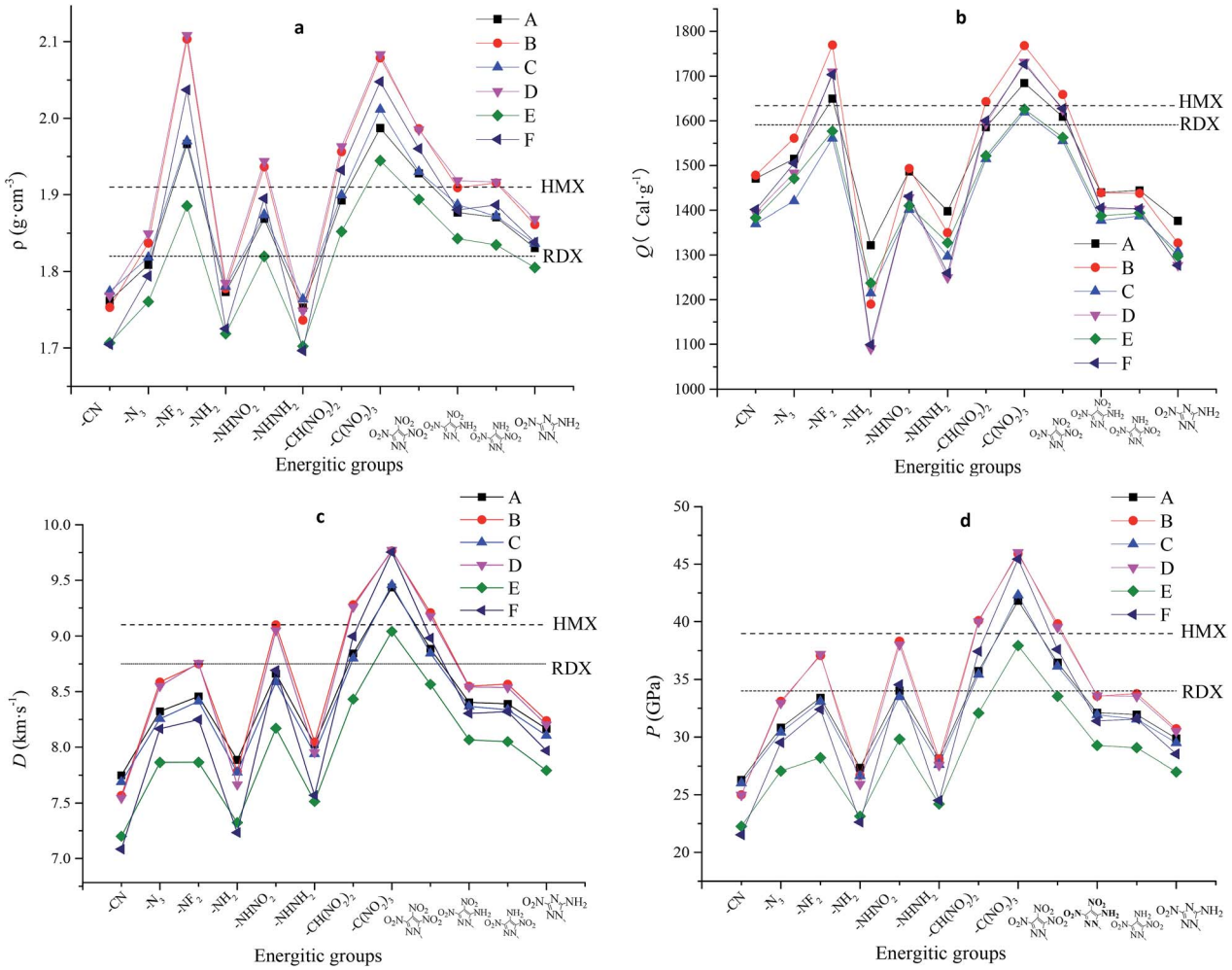

Fig. 3 (a–d) Variation trends of ρ, Q, D and P of designed compounds.

BDE is selected as the breaking bond based on bond order analyses. The bond order and BDEs (specific data are shown in ESI Table S3†) of all designed compounds were summarized and listed in Table 6. In most cases, the possible trigger bond was likely C–NO_2 in 3- or 5-position of the pyridine ring (such as **A1**, **A2**, **A9**). In particular, when trinitromethyl or dinitromethyl was incorporated to the pyridine ring, C–N bond in aliphatic carbon chain was weaker than that of aromatics (such as **A7**, **A8**). When N–NO_2 or N–NH_2 occurred, they both appeared to be the weakest bond in one curtain designed molecule. The nitrogen atom and fluorine atom both have strong ability to attract electron, making N–F bond broken more easily. It is shocking that N–H bond were known as the trigger bond in compound **A4** and **B4**, for example, which were contradictory with the concept of increasing thermal stability by the use of an alternating array of amino and nitro-groups. The results show that a p-π conjugation effect formed between the nitrogen atom and pyridine ring, revealing that the nitrogen atom has the weaker ability to attract the hydrogen atom. The ultimate cause of this situation seems to have been the steric hindrance effect between four nitro groups directly attached to the pyridine ring. Besides, incorporating the bridge –N=N– (series **A** and **B**) or –CH=CH– (series **E** and **F**) leads to the formation of π–π conjugation between double bonds and the pyridine ring, so as to stabilize the bridged atoms.

2.5 Thermal dynamic properties

As the main contents of thermal dynamic parameters, standard molar heat capacity ($C^{\theta}_{p,m}$), standard molar entropy (S^{θ}_{m}) and standard molar enthalpy (H^{θ}_{m}) can provide useful information in state equation, macroscopic properties and chemical reactions of energetic materials.[16] The variation trends of $C^{\theta}_{p,m}$, S^{θ}_{m} and H^{θ}_{m} of designed compounds at different temperatures (every 10 K from 200 K to 600 K, specific data are shown in ESI Table S4†) were investigated. The related equation for these parameters at different temperatures can be written in the following form:

Open Access Article. Published on 19 November 2019. Downloaded on 12/9/2025 12:19:22 AM.
This article is licensed under a Creative Commons Attribution-NonCommercial 3.0 Unported Licence.

Table 6 Bond dissociation energies (BDE, kJ mol^{-1}) for the weakest bonds

	C–N		N–N		N–H		N–F				C–N		N–N		N–H		N–F		
Compd	BO	BDE	BO	BDE	BO	BDE	BO	BDE	h_{50}	Compd	BO	BDE	BO	BDE	BO	BDE	BO	BDE	h_{50}
A1	0.676	252.8							35.1	**D1**					0.624	390.6			29.4
A2	0.67	262.5							54.3	**D2**					0.687	384.4			56
A3							0.137	230.6	34.5	**D3**							0.14	225.6	7.7
A4					0.677	444.5			50.3	**D4**					0.605	383.8			55.7
A5			0.57	180.1					32.4	**D5**			0.531	191.1					32.7
A6			0.61	315.8					54.8	**D6**					0.603	384.3			55.3
A7	0.539	183.4							19	**D7**	0.526	182.3							13.4
A8	0.457	174.4							11.9	**D8**	0.448	163.9							3.9
A9	0.674	269							25.3	**D9**					0.637	375.4			12.2
A10			0.614	279.1					40.9	**D10**			0.612	278					24.8
A11	0.671	256.6							46.9	**D11**					0.624	375.4			45.5
A12			0.655	297.9					49.3	**D12**			0.629	285.8					38.8
B1	0.687	252.2							24.7	**E1**	0.667	279.2							39.3
B2	0.677	269.3							54.1	**E2**	0.673	261.6							46
B3							0.139	229	29.4	**E3**							0.142	228.7	17.7
B4					0.667	449.8			53.9	**E4**					0.671	443.2			55.9
B5			0.546	183.5					27.8	**E5**			0.568	183.3					40.8
B6			0.619	318.9					53.2	**E6**			0.626	302.2					55.6
B7	0.526	181.8							11.8	**E7**	0.524	186.6							22.2
B8	0.453	173.6							3.9	**E8**	0.463	163.8							14.8
B9	0.668	239.4							12.4	**E9**	0.665	278.8							26.6
B10			0.585	266.1					22.8	**E10**			0.618	281					46.6
B11					0.673	442.6			43.9	**E11**	0.67	263							48.5
B12			0.619	281.6					42.6	**E12**			0.649	295.2					52.7
C1					0.632	402.9			40.2	**F1**	0.681	260							25.9
C2					0.628	405.4			53.4	**F2**	0.675	271.2							50.9
C3					0.626	380.1			21.4	**F3**							0.138	227.6	10.6
C4					0.616	382.3			52.7	**F4**					0.669	462.8			56
C5			0.556	182.8					35.1	**F5**			0.559	187.5					36.7
C6			0.609	324.4					56	**F6**			0.62	323.6					56.3
C7	0.53	186.1							19.6	**F7**	0.525	185.2							13
C8	0.463	169.8							14.9	**F8**	0.455	175.7							3.8
C9					0.626	380.5			25.9	**F9**	0.674	275.3							12.3
C10					0.624	394.6			45.3	**F10**			0.591	268.5					23.9
C11					0.629	379.6			46.4	**F11**					0.672	446.7			44.4
C12					0.625	394.9			48.3	**F12**			0.629	286.1					44.8

$$X = a + bT + \text{dis}\ cT^2\ (X = C^{\theta}_{\text{p,m}},\ S^{\theta}_{\text{m}} \text{ and } H^{\theta}_{\text{m}})$$

where a, b and c were constant and summarized in Table 7. Take compound **A1** and **A2** for example, as can be seen from Fig. 4, $C^{\theta}_{\text{p,m}}$, S^{θ}_{m} and H^{θ}_{m} of all designed compounds improved as the temperature increasing. However, there exists differences in the growth rates of these parameters. The case is that the growth rates $C^{\theta}_{\text{p,m}}$, S^{θ}_{m} decreased evidently as the temperature increasing while growth rate of H^{θ}_{m} increased. The reason is that the translations and rotations of chemical bonds were the main influencing factors at a low while vibrational movement occurred and intensified at a high temperature. At certain temperature, it is also found that the values of these thermal dynamic parameters increase as the volume of energetic groups increasing. This phenomenon may be caused by the strong space steric effects of energetic groups. For example, the $C^{\theta}_{\text{p,m}}$, S^{θ}_{m} and H^{θ}_{m} of compound **A7** and **A8** are 382.2 J mol^{-1} K^{-1}, 746.8 J mol^{-1} K^{-1}, 68.8 kJ mol^{-1} and 406.2 J mol^{-1} K^{-1}, 782.6 J mol^{-1} K^{-1}, 73.2 kJ mol^{-1}, respectively (300k). Obviously, $C^{\theta}_{\text{p,m}}$, S^{θ}_{m} and H^{θ}_{m} of compound **A7** are lower than those of compound **A8**.

The scaling factor is 0.9888 for ZPE, 1.0062 for variation of enthalpy from 0 K to T and 1.0104 for entropy.[14]

2.6 Electrostatic potential

Electrostatic potential (ESP), which provides meaningful insight into charge distributions and intermolecular interaction on the molecular surface of designed compounds were fully investigated. The ESP mapped surfaces and the surface areas of designed compounds were plotted in Fig. 5, where significant surface local minima and maxima of ESP are represented in blue and red, respectively. From Fig. 5, it is found that the positive potential (red areas) mainly concentrates on the parent skeleton while the negative

 This journal is © The Royal Society of Chemistry 2019

Open Access Article. Published on 19 November 2019. Downloaded on 12/9/2025 12:19:22 AM.
This article is licensed under a Creative Commons Attribution-NonCommercial 3.0 Unported Licence.

Table 7 Calculated $C^{\theta}_{p,m}$, S^{θ}_{m}, and H^{θ}_{m} of designed compounds

	H^{θ}_{m}			S^{θ}_{m}			$C^{\theta}_{p,m}$			
Compd	*a*	*b*	$C \times 10^{-4}$	a	*b*	$C \times 10^{-4}$	*a*	*b*	$C \times 10^{-4}$	R^2
A1	−13.67	0.17	3.43	316.24	1.61	−5.84	66.83	1.27	−7.25	0.9999
A2	−14.27	0.18	3.66	325.37	1.71	−6.17	70.84	1.35	−7.64	0.9999
A3	−15.32	0.19	3.77	319.51	1.75	−6.29	62.71	1.43	−8.48	0.9999
A4	−12.84	0.15	3.72	294.40	1.53	−4.97	35.94	1.36	−7.71	0.9999
A5	−13.78	0.18	4.20	351.56	1.82	−6.19	60.51	1.52	−8.48	0.9999
A6	−13.07	0.17	4.02	317.23	1.70	−5.69	62.74	1.39	−7.30	0.9999
A7	−16.28	0.22	4.81	377.39	2.15	−7.54	88.02	1.71	−9.30	0.9999
A8	−23.61	0.28	5.21	353.52	2.53	−9.44	114.15	1.95	−11.30	0.9999
A9	−22.53	0.30	6.18	457.74	2.84	−10.20	123.00	2.22	−12.20	0.9999
A10	−23.04	0.27	6.17	384.24	2.69	−9.18	88.28	2.25	−12.70	0.9999
A11	−23.25	0.27	6.18	357.26	2.72	−9.29	66.62	2.28	−12.70	0.9999
A12	−18.78	0.23	5.54	376.74	2.34	−7.76	70.06	2.00	−11.10	0.9999
B1	−18.17	0.22	3.50	334.52	1.89	−7.53	100.10	1.36	−8.23	0.9999
B2	−19.47	0.24	3.98	351.63	2.08	−8.16	106.47	1.53	−9.09	0.9999
B3	−16.65	0.17	4.09	344.90	2.17	−8.48	97.69	1.67	−10.40	0.9999
B4	−16.65	0.17	4.09	280.65	1.73	−5.74	37.36	1.56	−9.16	0.9999
B5	−18.31	0.24	5.04	402.39	2.30	−8.20	86.93	1.87	−10.70	0.9999
B6	−17.37	0.21	4.71	321.91	2.07	−7.16	86.48	1.63	−8.59	0.9999
B7	−23.43	0.32	6.28	448.67	2.98	−10.90	141.26	2.25	−12.40	0.9999
B8	−37.47	0.44	7.07	410.61	3.74	−14.80	197.03	2.71	−16.20	0.9999
B9	−36.12	0.48	9.01	592.24	4.36	−16.30	211.88	3.27	−18.30	0.9999
B10	−36.04	0.42	8.99	469.33	4.05	−14.20	146.79	3.31	−18.80	0.9999
B11	−37.54	0.42	9.01	447.09	4.05	−14.20	143.92	3.33	−19.00	0.9999
B12	−28.17	0.33	7.77	442.25	3.32	−11.20	98.66	2.84	−16.10	0.9999
C1	−14.12	0.17	3.67	301.20	1.62	−5.59	51.87	1.36	−7.81	0.9999
C2	−14.62	0.18	3.90	317.79	1.72	−5.95	57.52	1.44	−8.16	0.9999
C3	−15.40	0.18	3.99	318.38	1.76	−6.07	49.68	1.52	−8.99	0.9999
C4	−12.85	0.14	3.99	273.86	1.52	−4.54	16.55	1.46	−8.25	0.9999
C5	−14.04	0.18	4.44	335.05	1.82	−5.89	44.90	1.61	−9.01	0.9999
C6	−13.06	0.15	4.32	291.35	1.68	−5.14	38.75	1.50	−7.93	0.9999
C7	−16.84	0.22	5.06	359.46	2.16	−7.29	72.97	1.80	−9.87	0.9999
C8	−24.15	0.27	5.48	318.83	2.53	−9.09	95.53	2.05	−11.90	0.9999
C9	−22.69	0.30	6.41	454.62	2.86	−10.00	110.83	2.31	−12.80	0.9999
C10	−23.31	0.27	6.42	371.62	2.69	−8.91	73.25	2.34	−13.20	0.9999
C11	−23.37	0.27	6.39	390.57	2.71	−9.07	78.71	2.33	−13.10	0.9999
C12	−18.71	0.22	5.81	353.64	2.33	−7.34	51.40	2.09	−11.60	0.9999
D1	−18.79	0.22	3.75	320.11	1.90	−7.25	83.47	1.47	−8.87	0.9999
D2	−19.61	0.23	4.23	338.98	2.09	−7.87	91.89	1.62	−9.57	0.9999
D3	−21.61	0.24	4.40	328.94	2.18	−8.19	80.65	1.77	−11.10	0.9999
D4	−16.07	0.16	4.40	262.33	1.70	−5.15	12.66	1.67	−9.75	0.9999
D5	−18.11	0.23	5.33	388.11	2.30	−7.77	66.44	1.97	−11.30	0.9999
D6	−16.07	0.20	5.02	315.42	2.04	−6.56	64.90	1.72	−8.96	0.9999
D7	−24.23	0.31	6.53	424.35	2.98	−10.60	124.57	2.35	−13.00	0.9999
D8	−37.69	0.43	7.31	404.55	3.75	−14.50	181.19	2.81	−16.80	0.9999
D9	−36.03	0.47	9.25	587.67	4.37	−16.00	197.90	3.35	−18.70	0.9999
D10	−36.95	0.42	9.18	449.95	4.08	−14.20	140.18	3.38	−19.20	0.9999
D11	−37.67	0.42	9.24	443.85	4.07	−14.00	130.66	3.42	−19.60	0.9999
D12	−29.21	0.33	7.98	417.04	3.35	−11.10	88.59	2.93	−16.60	0.9999
E1	−12.46	0.17	3.65	329.32	1.61	−5.60	59.19	1.32	−7.32	0.9999
E2	−13.74	0.18	3.90	330.14	1.72	−5.92	61.45	1.41	−7.84	0.9999
E3	−13.05	0.18	3.96	354.61	1.76	−6.12	63.25	1.45	−8.15	0.9999
E4	−11.93	0.14	3.96	296.80	1.53	−4.66	25.02	1.43	−7.89	0.9999
E5	−13.25	0.18	4.43	348.30	1.82	−5.91	50.65	1.58	−8.65	0.9999
E6	−12.68	0.16	4.26	312.81	1.71	−5.44	50.83	1.47	−7.68	0.9999
E7	−16.12	0.22	5.05	368.84	2.16	−7.29	78.45	1.77	−9.50	0.9999
E8	−23.01	0.27	5.44	355.09	2.54	−9.20	106.03	2.00	−11.40	0.9999
E9	−21.50	0.29	6.41	468.24	2.85	−9.93	114.80	2.27	−12.30	0.9999
E10	−21.82	0.27	6.40	408.30	2.69	−8.91	79.88	2.30	−12.70	0.9999
E11	−22.17	0.27	6.40	397.63	2.70	−8.96	81.77	2.30	−12.70	0.9999
E12	−18.63	0.22	5.77	374.58	2.34	−7.51	59.98	2.06	−11.30	0.9999
F1	−17.15	0.22	3.72	337.71	1.89	−7.28	93.04	1.41	−8.26	0.9999

Open Access Article. Published on 19 November 2019. Downloaded on 12/9/2025 12:19:22 AM.
This article is licensed under a Creative Commons Attribution-NonCommercial 3.0 Unported Licence.

Table 7 (*Contd.*)

	H_m^θ			S_m^θ			$C_{p,m}^\theta$			
Compd	*a*	*b*	$C \times 10^{-4}$	a	*b*	$C \times 10^{-4}$	*a*	*b*	$C \times 10^{-4}$	R^2
F2	−18.75	0.23	4.22	357.10	2.09	−7.89	96.91	1.59	−9.25	0.9999
F3	−19.10	0.24	4.39	372.18	2.17	−8.16	90.36	1.71	−10.30	0.9999
F4	−15.95	0.16	4.34	279.41	1.73	−5.40	24.56	1.63	−9.41	0.9999
F5	−17.51	0.24	5.28	408.60	2.31	−7.90	75.88	1.93	−10.90	0.9999
F6	−16.23	0.20	4.96	320.00	2.06	−6.80	75.92	1.69	−8.65	0.9999
F7	−23.28	0.31	6.53	445.24	2.98	−10.60	129.40	2.32	−12.70	0.9999
F8	−36.86	0.43	7.30	411.23	3.74	−14.50	187.82	2.77	−16.30	0.9999
F9	−35.17	0.47	9.22	597.80	4.37	−16.00	207.33	3.30	−18.20	0.9999
F10	−34.88	0.42	9.16	498.70	4.07	−14.20	148.64	3.33	−18.60	0.9999
F11	−36.47	0.42	9.23	462.29	4.06	−14.00	136.87	3.38	−19.10	0.9999
F12	−27.23	0.33	8.00	444.36	3.32	−10.90	89.91	2.89	−16.10	0.9999

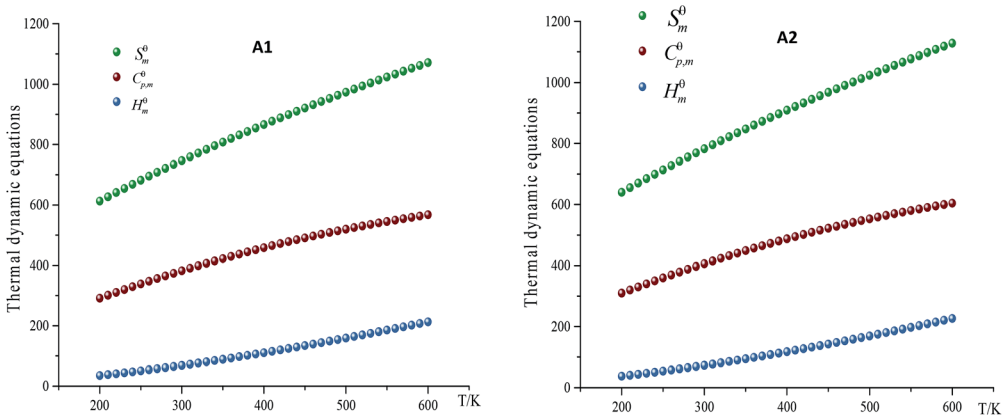

Fig. 4 Relationships between the thermodynamic equations and temperature for compound **A1** and **A2**.

potential (blue areas) distributed mostly on the nitro groups and difluoramino groups, especially on the fluorine atom, which mainly due to its higher electronegativity. The positive areas of compounds **B1**, **B2**, **B3**, **B4**, **B5**, **B8**, **B9** and **B12** were calculated as 248 Å^2 (ratio 61%), 251 Å^2 (ratio 57%), 218 Å^2 (ratio 56%), 180 Å^2 (ratio 51%), 272 Å^2 (ratio 58%), 398 Å^2 (ratio 63%), 549 Å^2 (ratio 65%), 426 Å^2 (ratio 62%) respectively. As we can see that the positive regions are larger but also stronger in magnitude than the negative ones, which is consistent with Murray's research.[17] Generally speaking, for organic molecules the negative regions cover a smaller portion of the total surface area but are significantly stronger (in terms of average magnitudes) than the positive ones. However, in the case of energetic molecules, the positive regions are not only larger but also stronger than the negative ones. From Table 6, the h_{50} values of compounds **B1**, **B2**, **B3**, **B4**, **B5**, **B8**, **B9** and **B12** were calculated as 24.7 J, 54.1 J, 29.4 J, 53.9 J, 27.8 J, 3.9 J, 12.4 J, 42.6 J respectively. It is interesting to find that the surface electrostatic potentials of the less sensitive molecules do not differ dramatically from those of the others. The delocalization of the π electronic charge that is such an important factor in stabilizing aromatic systems is counteracted in the nitroaromatics by the strongly electron-withdrawing effect of NO_2 groups, which is reflected in the surface electrostatic potentials being positive rather than negative above the rings and in high degrees of internal charge separation.[18] As a result, positive areas of designed compounds were higher than negative areas which may stabilize the molecular structure.

3 Conclusions

In this work, a series of bridged pyridine energetic derivatives were designed and investigated by density functional theory method at DFT-D3(BJ)/B3LYP/6-311G(d,p) level. The results show that steric hindrance effect is a decisive factor for structural stability, and formation of intramolecular or intermolecular hydrogen bonds doesn't have advantages to stabilize molecular structure. The azide group and azo bridge can improve heats of formation of energetic pyridine-based materials. Compound **D8** has the highest value of

Open Access Article. Published on 19 November 2019. Downloaded on 12/9/2025 12:19:22 AM.
This article is licensed under a Creative Commons Attribution-NonCommercial 3.0 Unported Licence.

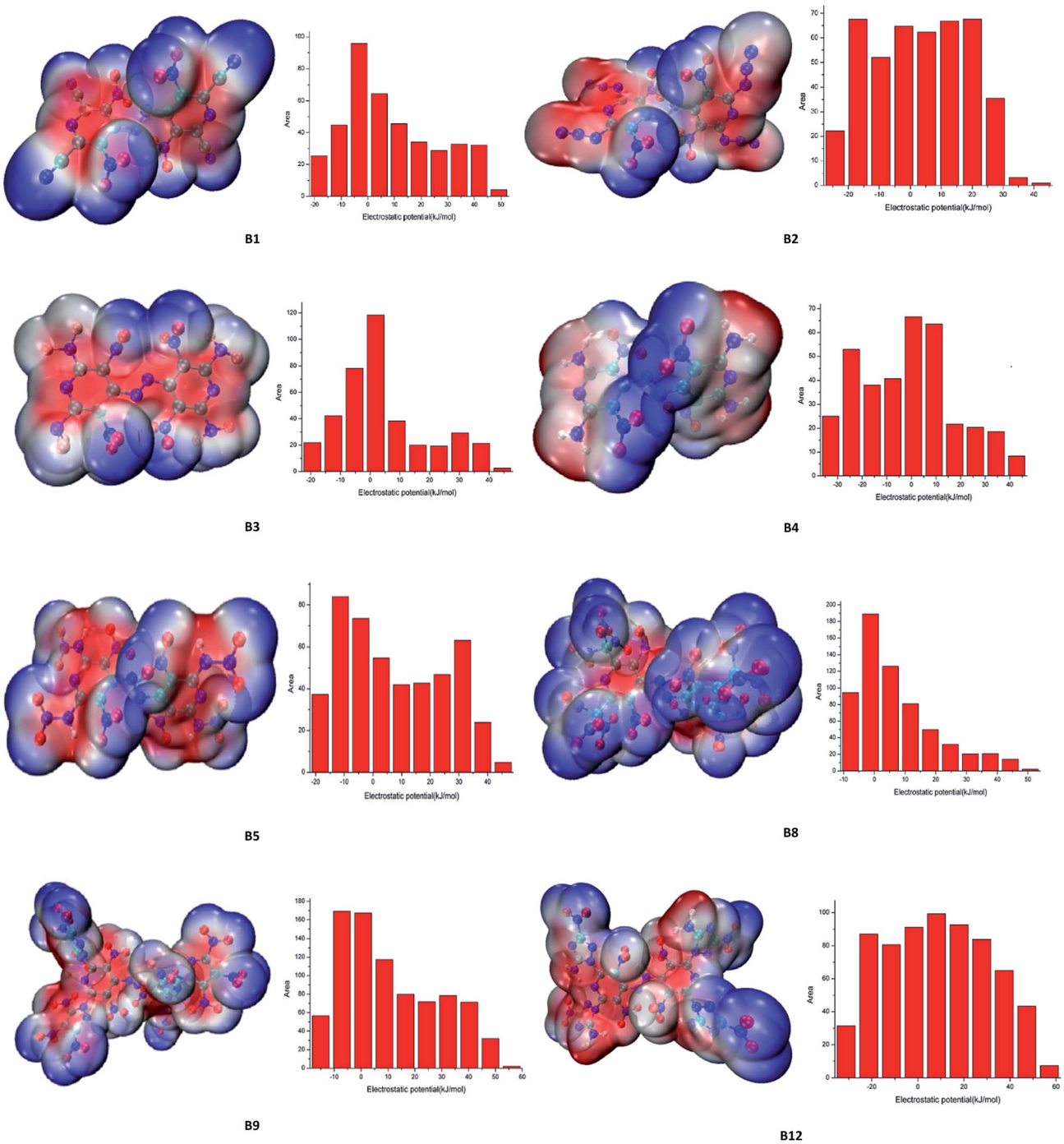

Fig. 5 Electrostatic potential of representative designed molecules.

detonation velocity (9.77 km s^{-1}) and detonation pressure (46.0 GPa), which is better than that of **RDX** and **HMX**, and can be selected as a potential candidate of promising high energy density materials. Analysis of the bond dissociation energies suggests that When a p-π conjugation formed between the nitrogen atom and pyridine ring, the bond between nitrogen and hydrogen atoms may be broken as the trigger bond.

Conflicts of interest

There are no conflicts of interest to declare.

Acknowledgements

This study was supported by the National Natural Science Foundation of China (No. 11702129). We are so grateful to the

Open Access Article. Published on 19 November 2019. Downloaded on 12/9/2025 12:19:22 AM.
This article is licensed under a Creative Commons Attribution-NonCommercial 3.0 Unported Licence.

High Performance Computing Center of Nanjing Tech University for doing the numerical calculations in this paper on its x-Flex enterprise blade cluster system.

Notes and references

1 P. F. Pagoria, G. S. Lee, A. R. Mitchell and R. D. Schmidt, *Thermochim. Acta*, 2002, **384**, 187–204.
2 M. A. Hiskey, N. Goldman and J. R. Stine, *J. Energ. Mater.*, 1998, **16**, 119–127.
3 H. H. Licht and H. Ritter, *Propellants, Explos., Pyrotech.*, 1988, **13**(1), 25–29.
4 H. Ritter and H. H. Licht, *J. Heterocycl. Chem.*, 1995, **32**, 585–590.
5 K. Zhao, Z. L. Liu and C. M. Ma, *Chin. J. Energy Mater.*, 2015, **23**, 1099–1102.
6 C.-M. Ma, Z. L. Liu and Q. Z. Yao, *Chin. J. Energy Mater.*, 2015, **23**, 1176–1180.
7 Y. Chen, H. X. Hao, S. Y. Xu and W. F. Zheng, *J. Ordnance Equip. Eng.*, 2017, **38**(6), 125–134.
8 A. Stobiecka, M. Sikora, R. Bonikowski and J. Kula, *J. Mol. Struct.*, 2016, **1107**, 82–90.
9 K. E. Gutowski, R. D. Rogers and D. A. Dixon, *J. Phys. Chem. B*, 2007, **111**, 4788–4800.
10 E. A. Miroshnichenko, T. S. Kon'kova and Y. N. Matyushin, *Dokl. Phys. Chem.*, 2003, **392**, 253–255.
11 Á. Furka, *Struct. Chem.*, 2009, **20**, 605–616.
12 W. N. Hubbard, F. R. Frow and G. Waddington, *J. Phys. Chem.*, 1961, **65**, 1326–1328.
13 P. Jiménez, M. V. Roux and C. Turrión, *J. Chem. Thermodyn.*, 1989, **21**, 759–764.
14 J. P. Merrick, D. Moran and L. Radom, *J. Phys. Chem. A*, 2007, **111**, 11683–11700.
15 M. B. Talawar, R. Sivabalan, T. Mukundan, H. Muthurajan, A. K. Sikder, B. R. Gandhe and A. S. Rao, *J. Hazard. Mater.*, 2009, **161**, 589–607.
16 J. Zhang and H. Xiao, *J. Chem. Phys.*, 2002, **116**, 10674–10683.
17 J. S. Murray, P. Lane and P. Politzer, *Mol. Phys.*, 1998, **93**, 187–194.
18 J. S. Murray, P. Lane and P. Politzer, *Mol. Phys.*, 1995, **85**, 1–8.

 This journal is © The Royal Society of Chemistry 2019